Adaptive least-squares RTM and application to Freedom WAZ subsalt imaging

Chong Zeng, Shuqian Dong, Zhaohong Wu, Jean Ji, Darrell Armentrout, and Bin Wang, TGS*

Summary

We propose an adaptive approach to address the practical issues in least-squares reverse time migration (LSRTM) with a focus on subsalt imaging. The problems include imperfect migration velocity, slow convergence in subsalt area, and extra migration artifacts introduced in gradient computation. The adaptive solution involves strategies to enhance data consistency in time domain and control the migration aperture to precondition the LSRTM gradient for fast convergence. We use constrained dynamic warping to correct the misalignments between synthetic and input waveforms due to short-wavelength velocity errors. The waveform amplitude differences are mitigated by a locally windowed gain using input data as reference. During the LSRTM iterations we gradually open the migration aperture to control the weighting for updating structures with different dips. The extra artifacts introduced during gradient computation by the two-way migration operator are suppressed via a structure-oriented smoothing process. We demonstrate the effectiveness of the proposed adaptive strategies via a 3D synthetic model derived from the true geology of the Gulf of Mexico (GoM). Lastly, we examine the results of the adaptive LSRTM approach on our multi-client wide-azimuth data acquired in the Freedom area of the GoM. The images of shadow zone and subsalt area are significantly improved after a few iterations regardless of the practical limitations such as velocity error and weak illumination near and below the salt body.

Introduction

Seismic imaging algorithms are continuously evolving and the corresponding research is moving toward inversion-based methods such as least-squares migration (LSM, [Schuster, 1993, Nemeth et al., 1999, Duquet et al., 2000, and Tang, 2009]). Least-squares reverse time migration (LSRTM) has gained particular interest in recent years (e.g., Wong et al., 2011, Dong et al., 2012, Dai et al., 2013, Zhang et al., 2013, and Zhan et al., 2014) by virtue of its improved amplitude response, higher spatial resolution, reduced migration artifacts, and enhancement of complex structures (Zeng et al., 2014a) compared to conventional depth migration algorithms. Despite the encouraging success of LSRTM on preliminary field data studies, further investigation is needed to address many practical issues such as unknown source wavelet, imperfect migration velocity, massive computation cost, etc. Appropriate quality control (QC) methods are also needed to ensure the convergence of LSRTM iterations or to uncover the problems as early as possible when the inversion is unstable. Sophisticated strategies are also needed to improve the stability of LSRTM so that it can be less prone to the practical problems in conventional depth migration.

In general, LSRTM iteratively updates the seismic image with a similar workflow to what is used in full waveform inversion (FWI). One of the major differences between these two methods with respect to implementation is that LSRTM searches for solution based on seismic reflectivity rather than seismic velocity in FWI. Currently all LSRTM algorithms are implemented as a single parameter inversion for seismic reflectivity (or impedance) only, in which seismic velocity is fed to the program as an input parameter and remains unchanged during the entire inversion procedure. This raises a fundamental problem of LSRTM: any errors in the velocity model will propagate throughout the inversion and will introduce uncertainty in the final inverted seismic image. From this point of view, LSRTM encounters the same paradox related to the requirement of seismic velocity in conventional depth migration algorithms. In theory LSRTM has to assume the velocity model is perfect otherwise there will be time shifts between the waveforms of synthetic and input data. This misalignment distorts the subtracted residual waveforms, and then smear the gradient after back projection using the same migration kernel. In previous studies (e.g. Wang et al., 2013, Dong et al., 2014, Zeng et al., 2014a, and Zeng et al., 2014b) a matching filter was applied to the synthetic data to partially correct this problem. Also, Luo and Hale (2014) proposed to warp the input data rather than synthetic data to force the time domain data and the migrated depth domain image to be consistent. Here we revise this approach with a more sophisticated quality control to raise the confidence level of the warped data. The concept of this data warping strategy is coincident with the "adaptive image focusing" idea proposed by Etgen et al. (2014). Therefore, we name our approach "adaptive LSRTM" because the input data are adaptively corrected to compensate for the velocity errors.

Furthermore, we extend the concept of adaptive imaging by altering migration parameters (such as aperture) during LSRTM iterations to speed up the convergence of the inversion focusing on subsalt area. This approach is efficient particularly when interpreters are more interested in the subsalt geology of the sediments related to potential reservoirs. We name this an "image adaptive" strategy because it is equivalent to applying natural weights to sediment images which are gently dipping in subsalt areas. Computation cost will also be greatly reduced due to the controlled aperture in LSRTM. To eliminate the extra artifacts generated by the two-way migration operator

DOI http://dx.doi.org/10.1190/segam2015-5916514.1

during gradient computation, we apply a structure-oriented smoothing (Fehmers and Höcker, 2003, and Hale, 2009) to clean up the stacked gradient so that the subsalt image can be updated without introducing extra migration swings.

In the following paragraphs, we discuss the proposed adaptive strategies in detail. We also demonstrate the effectiveness of the adaptive strategies via synthetic and real world examples based on data from the GoM.

Data Adaptive with Constrained Dynamic Warping

By realizing the challenges of velocity model building with increased geological complexity, it is expected that the migration velocity is never perfect in practice (Etgen et al., 2014). An interesting study presented by Albertin and Zhang (2014) shows that migration error occurs even with perfect velocity model when a complex salt body involved. The convergence of LSRTM is measured by minimizing the least-squares difference between synthetic and input seismic waveforms. In theory, this waveform difference should be related only to the difference between migrated seismic image and the true earth reflectivity. However, the almost unavoidable velocity errors violate this assumption and introduce unwanted time shifts in synthetic waveforms with respect to the input data. Previously, we used a matching filter to correct the synthetic data so that the waveforms can be aligned to generate reasonable residual waveforms. However, this correction will be cancelled when we reverse-time migrate the residual and generate a blurred gradient due to using inaccurate velocities (again) for migration. It is attractive to apply a local wavefield correction in image domain before stacking (e.g., Huang et al., 2014, Etgen et al., 2014, and Albertin and Zhang, 2014) to re-focus the image. An equivalent data domain method is to adjust the input data to force it to be consistent with the velocity model and the migrated image (Luo and Hale, 2014). For LSRTM this data domain adjustment is feasible because it is done only once before the first iteration. Thus, imposing no extra computation cost for the inversion. Because the modeling kernel and the migration kernel share the same velocity model, the synthetic data are self-consistent with the migrated image in terms of time to depth mapping. After adjusting the input data using synthetic as reference, we can obtain a better-focused image by correctly mapping the time-domain data to depth-domain image.

Similar to Luo and Hale (2014), we employ dynamic warping (Hale, 2013) to perform the adaptive data correction. We should be aware that dynamic warping itself assumes that the differences of the two input signals are minor and mainly due to (temporal or spatial) distortion. That means we need to assume that the seismic events in the synthetic data can be always found to match those in the reference data. However, in LSRTM, this is not always true due to the quality limitation of the initial image. Especially for the images near the salt, e.g. in the shadow zone or just below the base of salt, the image quality is usually limited compared to those in shallow sediments above the salt. In addition, extra artifacts on the initial image will also generate spurious events on the synthetic record and therefore degrade the coherency of the synthetic and input waveforms. To overcome this problem, we introduce a confidence level to measure the reliability of the warped data to evaluate the quality of the data adaptive correction. The confidence level at each sample point is calculated by a 2D normalized cross-correlation as follows:

$$c_i = \frac{\sum_{ix=-h}^{h}\sum_{it=-l}^{l}(d_i-\bar{d})(u_i-\bar{u})}{\sqrt{\sum_{ix=-h}^{h}\sum_{it=-l}^{l}(d_i-\bar{d})^2}\sqrt{\sum_{ix=-h}^{h}\sum_{it=-l}^{l}(u_i-\bar{u})^2}} \quad (1)$$

where d and u are the warped input and synthetic samples, respectively. The h and l correspond the half window size along the spatial and temporal direction.

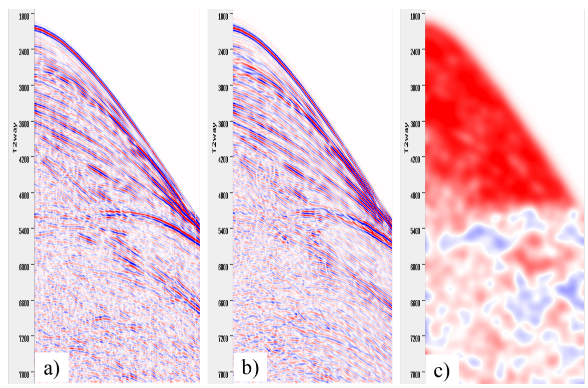

Figure 1. a) Input shot record, b) Synthetic shot record, and c) the confidence level for residual weighting based on cross correlation.

We measure the coherence of the warped input and the reference (synthetic) by calculating the confidence level using a 2D sliding window in *x-t* domain according to equation 1. A high confidence level indicates the input waveform matches the synthetic one well in the scale of the dominant period, while a low confidence level suggests the warping is inappropriate making the result less reliable. By using this confidence level to constrain the corresponding residual data, we can avoid unwanted artifacts in the gradient by automatically filtering out the less desirable residual waveforms. Figure 1 illustrates the concept of residual weighting based on the confidence level.

DOI http://dx.doi.org/10.1190/segam2015-5916514.1

After travel time adjustment of the input data by dynamic warping, we also need to correct the amplitude of the synthetic since it too will be inaccurate due to the limitation of Born modeling. It is noteworthy that in practical amplitude correction we should fix the synthetic amplitude only to a certain level rather than a perfect match. Otherwise, we will lose the true amplitude advantage of LSRTM. Specifically, an ideal amplitude match should produce waveforms that have same overall amplitude level in the scale of dominant period with only detailed differences that are meaningful to LSRTM. To accomplish this we employ a strategy of reference gain control which is related to automatic gain control (AGC). To preserve the true amplitude variation rather than equally scaling up everything, we first normalize the amplitude of synthetic waveforms. Then, we match the root-mean-square (RMS) value to that of the input waveform. After that, the residual can be obtained by direct subtraction of the input and synthetic waveforms with the weighting from the previously calculated confidence level.

Image Adaptive with Controlled Aperture

We extend the idea of adaptive imaging to the imaging domain for LSRTM with a focus on the subsalt. In structural imaging interpreters are more interested in the locations (or geometric shapes) of reflectors than the true amplitudes of the steep dips, such as faults or salt flanks. Conventional LSRTM is not explicitly aware of the dip information used by the two-way wave equation. It simply treats all events equally and updates them simultaneously during iterations. The salt body itself is a strong reflector that contributes more to the overall least-squares data misfit. Usually LSRTM uses the final velocity model in which the salt bodies are well defined by sophisticated model building processes. So, updating the images of salt bodies is not as important as fine tuning the sediments near or below the base of salt. The true amplitude information is usually focused on the relatively gently dipping subsalt sediments that are close to the salt body, where potential oil traps may exist. It is obvious that equal updating of all images, regardless of the geological emphasis, increases the number of iterations in efficiency. In many cases, the subsalt sediments are dipping relatively gently and can be imaged without a large aperture. By limiting the migration aperture when calculating the LSRTM gradient, we naturally drop the updates for steeply dipped salt flanks (since their amplitudes are less important as long as their location and shape remain intact) and concentrate more on the nearby, poorly-imaged sediments. This can greatly reduce the cost of LSRTM and speed up the convergence of the inversion to efficiently obtain satisfactory images for subsalt sediments. In practice, we first migrate the data using large (inline and cross-line) apertures to get good initial image containing well defined steep dips. Then we calculate the gradient starting with a relatively small aperture and gradually increase the aperture during each iteration of LSRTM updating. This strategy, in principle, is a natural (image domain) adaptive weighting process for LSRTM updating that recognizes the geological emphasis. The controlled aperture strategy benefits the inversion with respect to not only the subsalt image quality but also less computation cost.

We use total illumination compensation to scale up the LSRTM updates corresponding to the weak subsalt events for fast convergence. A side effect is the migration artifacts in the subsalt area are also boosted up. To eliminate these extra artifacts on the gradient we apply a structure-oriented smoothing to the stack gradient. We found this preconditioning is essential to the adaptive approach to properly enhance the image S/N in subsalt.

Examples

We test the adaptive strategies using a 3D synthetic model dominated by a salt body. Figure 2 shows the images of the near-salt sediments are closer to the true reflectivity after three LSRTM iterations. Finally, we apply the adaptive LSRTM to a WAZ real data from a subset of the Freedom area in the GoM. The success of the subsalt image improvements (Figure 3) confirms the effectiveness of the adaptive LSRTM strategies.

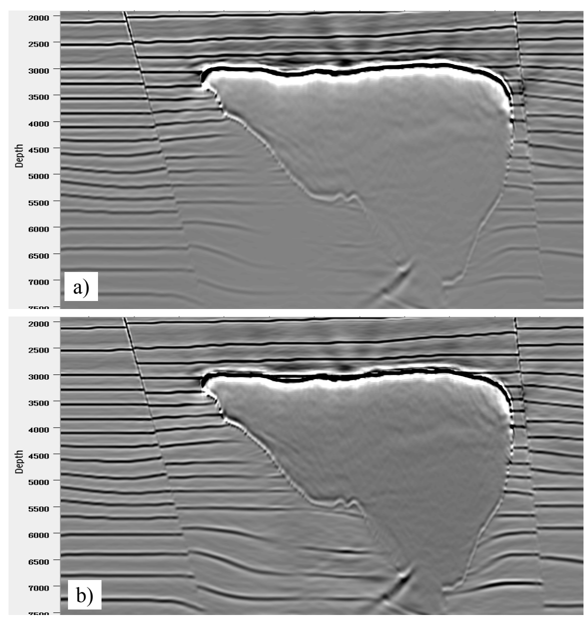

Figure 2. a) Conventional RTM, and b) Adaptive LSRTM images of the synthetic salt model based on the geology of the GoM.

DOI http://dx.doi.org/10.1190/segam2015-5916514.1

Conclusions

We present an adaptive approach and detailed strategies for LSRTM focusing on subsalt imaging. The adaptive LSRTM overcomes the practical issues such as short-wavelength velocity errors, amplitude mismatch, and slow convergence for subsalt events due to weak illumination. Both the synthetic and real data examples based on the GoM data show significant improvements for images near the steeply dipped salt flanks and those below the base of salt within just a few LSRTM iterations.

Acknowledgements

We are grateful to Davide Teixeira, Zhigang Zhang for their extraordinary efforts on GPU programming, and Sang Suh, James Sheng, Jian Mao, and Will Whiteside for helpful discussion. We also thank Connie VanSchuyver and Christopher Egger for the manuscript proof-reading. We greatly appreciate Zhiming Li, Terry Hart, George Cloudy, Gary Rodriguez, and Henrik Roende for their continuous support. At last, we thank TGS and WesternGeco for permission to show the Freedom data.

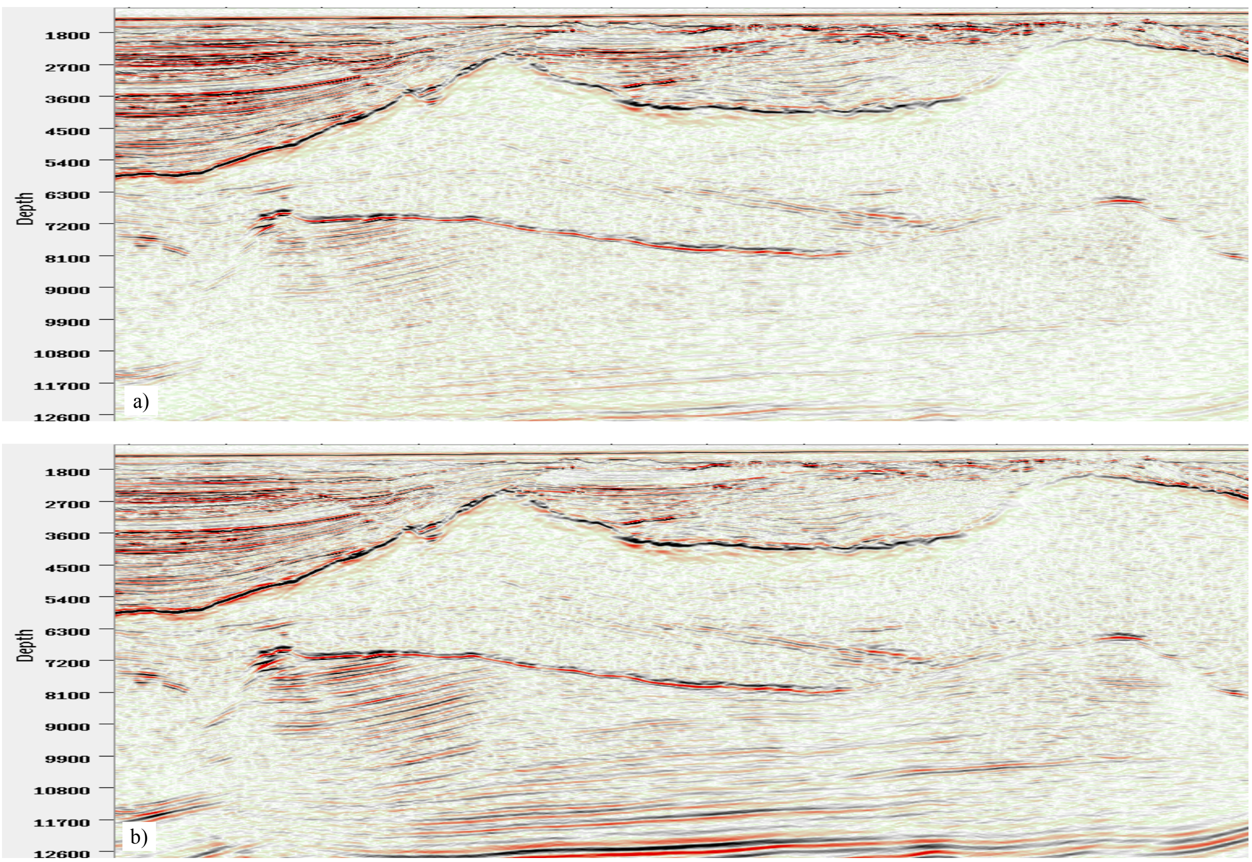

Figure 3. a) Conventional RTM, and b) Adaptive LSRTM images (two iterations) migrated from the Freedom WAZ data in the GoM.

DOI http://dx.doi.org/10.1190/segam2015-5916514.1

EDITED REFERENCES

Note: This reference list is a copyedited version of the reference list submitted by the author. Reference lists for the 2015 SEG Technical Program Expanded Abstracts have been copyedited so that references provided with the online metadata for each paper will achieve a high degree of linking to cited sources that appear on the Web.

REFERENCES

Albertin, U., and L. Zhang, 2014, Migration optimization through local phase alignment of partial migration images: 84th Annual International Meeting, SEG, Expanded Abstracts, 3769–3773. http://dx.doi.org/10.1190/segam2014-0805.1.

Dai, W., Y. Huang, and G. T. Schuster, 2013, Least-squares reverse time migration of marine data with frequency-selection encoding: Geophysics, **78**, no. 4, S233–S242. http://dx.doi.org/10.1190/geo2013-0003.1.

Dong, S., J. Cai, M. Guo, S. Suh, Z. Zhang, B. Wang, and Z. Li, 2012, Least-squares reverse time migration: Towards true amplitude imaging and improving the resolution: 82nd Annual International Meeting, SEG, Expanded Abstracts. http://dx.doi.org/10.1190/segam2012-1488.1.

Dong, S., C. Zeng, H. Masoomzadeh, and B. Wang, 2014, Deghosted Least-squares RTM: image domain broadband solution for complex structures: 76th Conference and Exhibition, EAGE, Extended Abstracts. http://dx.doi.org/10.3997/2214-4609.20141449.

Duquet, B., K. J. Marfurt, and J. A. Dellinger, 2000, Kirchhoff modeling, inversion for reflectivity, and subsurface illumination: Geophysics, **65**, no. 4, 1195–1209. http://dx.doi.org/10.1190/1.1444812.

Etgen, J. T., C. Chu, T. Yang, and M. Vyas, 2014, Adaptive image focusing: 84th Annual International Meeting, SEG, Expanded Abstracts, 3774–3778. http://dx.doi.org/10.1190/segam2014-0820.1.

Fehmers, G. C., and C. F. W. Höcker, 2003, Fast structural interpolation with structure-oriented filtering: Geophysics, **68**, no. 4, 1286–1293. http://dx.doi.org/10.1190/1.1598121.

Hale, D., 2009, Structure-oriented smoothing and semblance: CWP report 635, 1-10.

Hale, D., 2013, Dynamic warping of seismic images: Geophysics, **78**, no. 2, S105–S115. http://dx.doi.org/10.1190/geo2012-0327.1.

Huang, Y., X. Wang, and G. T. Schuster, 2014, Nonlocal means filter for trim statics: 84th Annual International Meeting, SEG, Expanded Abstracts, 3925–3929. http://dx.doi.org/10.1190/segam2014-0352.1

Luo, S., and D. Hale, 2014, Least-squares migration in the presence of velocity errors: 84th Annual International Meeting, SEG, Expanded Abstracts, 3980–3984. http://dx.doi.org/10.1190/segam2014-1367.1.

Nemeth, T., C. Wu, and G. T. Schuster, 1999, Least-squares migration of incomplete reflection data: Geophysics, **64**, no. 1, 208–221. http://dx.doi.org/10.1190/1.1444517.

Schuster, G. T., 1993, Least-squares crosswell migration: 63rd Annual International Meeting, SEG, Expanded Abstracts, 110–113. http://dx.doi.org/10.1190/segam2012-1425.1.

Tang, Y., 2009, Target-oriented wave-equation least-squares migration/inversion with phase-encoded Hessian: Geophysics, **74**, no. 6, WCA95–WCA107. http://dx.doi.org/10.1190/1.3204768.

Wang, B., S. Dong, and S. Suh, 2013, Practical aspects of least-squares reverse time migration: 75th Conference and Exhibition, EAGE, Extended Abstracts. http://dx.doi.org/0.3997/2214-4609.20131000.

Wong, M., S. Ronen, and B. Biondi, 2011, Least-squares reverse-time migration/inversion for ocean bottom data: A case study: 81st Annual International Meeting, SEG, Expanded Abstracts, 2369–2373. http://dx.doi.org/10.1190/1.3627684.

Zeng, C., S. Dong, and B. Wang, 2014a, Least-squares reverse time migration: inversion-based imaging toward true reflectivity: The Leading Edge, **33**, 962–968. http://dx.doi.org/10.1190/tle33090962.1.

Zeng, C., S. Dong, J. Mao, and B. Wang, 2014b, Broadband least-squares reverse time migration for complex structure imaging: 84th Annual International Meeting, SEG, Expanded Abstracts, 3715–3719. http://dx.doi.org/10.1190/segam2014-1283.1.

Zhan, G., W. Dai, M. Zhuo, Y. Luo, and G. T. Schuster, 2014, Generalized diffraction-stack migration and filtering of coherent noise: Geophysical Prospecting, **62**, no. 3, 427–442. http://dx.doi.org/10.1111/1365-2478.12086.

Zhang, Y., L. Duan, and Y. Xie, 2013, A stable and practical implementation of least-squares reverse time migration: 83rd Annual International Meeting, SEG, Expanded Abstracts, 3716–3720. http://dx.doi.org/10.1190/segam2013-0577.1.

DOI http://dx.doi.org/10.1190/segam2015-5916514.1